Joint Position and Clock Tracking of Wireless Nodes

Juan Pablo Grisales Campeón[a], Pablo I. Fierens[a,b]

[a] *Instituto Tecnológico de Buenos Aires (ITBA), Ciudad de Buenos Aires, C1106ACD Argentina*
[b] *Consejo Nacional de Investigaciones Científicas y Técnicas (CONICET), Ciudad de Buenos Aires, C1425FQB Argentina*

Abstract

In this paper we consider the problem of joint position and clock tracking of a mobile wireless node by a set of reference nodes. Imperfections of the mobile clock are characterized by its skew and offset, which are assumed to change with time according to simple random walk models.

We put forth a measurement protocol, similar to that used in two-way ranging, and apply extended and unscented Kalman filters to estimate the position and the velocity of the mobile, and the skew and offset of its clock. We analyze the performance of the algorithms by means of extensive simulations, where the mobile's velocity is assumed to follow a random walk. Simulation results are compared to the Cramér-Rao bound for a simplified model of a mobile with constant velocity.

We show that estimation errors are largely independent of the mean values of the offset and the skew, but they increase with the mean speed. We also study how estimation errors are influenced by other factors such as the number of reference nodes.

We believe these results to be of relevance, specially, in indoor positioning applications.

Keywords: Joint estimation, synchronization, tracking, clock.

1. Introduction

Localization of wireless devices is an essential capability enabling other applications such as personnel and asset tracking, factory automation, workplace safety, Internet-of-Things, wireless network security, location-based advertising, location services for vehicles and traffic management [1–3].

The Global Positioning System (GPS) is probably the most extended technology for localization and tracking, but it is not suitable for every application and its precision degrades in urban or indoors environments [1, 4]. Multiple technologies like Bluetooth beacons, magnetic field signatures, and received signal strength (RSS) from WiFi or 3GPP transmitters have been used in these scenarios [5–9]. In particular, many popular commercial approaches to indoor positioning are based on the use of WiFi RSS signatures known as *fingerprints*.

Several regression algorithms have been proposed to match these fingerprints to actual site positions. The overall accuracy of these techniques is in the order of 1 m [10, 11]. One of their main drawbacks is the need for an initial laborious calibration phase. Moreover, changes in the placement of furniture, addition or removal of walls and other environmental changes may render the fingerprints outdated and inaccurate. These problems have led to the development of zero-calibration, unsupervised positioning algorithms using RSS [12, 13].

There is a vast literature, as well as many commercial products, on positioning approaches based on the time of arrival of wireless signals (see, e.g., [4, 14, 15] and references therein), as they have better accuracy than RSS-based positioning systems [13, 16, 17]. However, these approaches also face many challenges. Particularly, there are many sources of timing error such as multipath fading [18–21], multiuser interference [22, 23], non-line-of-sight propagation [24–28], timing jitter [29], clock offset and drift [30].

The focus of this paper is on positioning systems based on time of arrival (ToA) of wireless signals. Specifically, we propose algorithms that enable the simultaneous estimation of the position, velocity, clock offset and drift of a mobile node based on imperfect time measurements. In order to understand the problem, let us review some basic concepts of time-based ranging and positioning. First, we must note that *absolute* synchronization is not required. Indeed, it is well known that absolute synchronization is unnecessary for positioning when time difference of arrivals (TDoA) is used [16, 17, 31–33]. Another way of avoiding absolute synchronization is by means of two-way ranging (TWR) [4], which is the core of the proposal in this work. In order to understand the basics of TWR, let us assume that we wish to estimate the distance between nodes A and B which are not synchronized and time measured at A (t_A) is related to time measured at B (t_B) by $t_A = t_B +$, where is an unknown offset between the clocks at A and B. In two-way ranging, node A sends a message and B replies *immediately*. Node A can estimate the distance to B from the round trip time (RTT). Since sending and arrival times are measured locally at A, the offset does not influence the RTT measurement and the range estimation. However, if the clock at A drifts [34–36], the measured round trip time can be either shorter or longer than the actual RTT leading to under or overestimate of the distance to B.

A common supposition is that A's clock is perfect, but the clock at B may drift. This is a reasonable assumption in a setup with costly reference nodes (A) and cheaper mobile nodes (B). Nonetheless, even in this case there are errors in the measurement of the round trip time. Indeed, in practice node B does not reply immediately as there is a necessary processing time. It is through this processing time that B's clock inaccuracies introduce errors in the RTT measurement (see Eq. (6) in Section 3.4). In order to improve the ranging accuracy, B's clock drift needs to be estimated.

There are many works in the literature on the joint positioning and synchronization problem (see Section 2). However, the proposal in this paper stands out as the only one, to the best of our knowledge, that meets the following criteria:

- There are a number of perfectly synchronized, stationary reference nodes, also known as *anchors*, and a mobile node with an imperfect clock.
- Drift and offset of the mobile node's clock change.
- Velocity of the mobile node also changes.
- The message processing time at the mobile node is explicitly taken into account.
- Position and velocity of the mobile node and the drift and offset of its clock are tracked online. That is, these parameters are not estimated offline with a batch processing algorithm.
- Ranging is not required for the estimation of position and velocity.

Since we use standard estimation techniques, such as extended and unscented Kalman filters (see Section 4), the novelty of our work is not in these algorithms, but on the comprehensive approach to the problem. Moreover, the explicit inclusion of the processing time at the mobile node requires a modification of the usual two-way ranging methodology. Indeed, we describe an original and complete protocol in Section 3.4.

The remaining of the paper is organized as follows. We briefly review the related literature in Section 2. In Section 3 we describe the modeling framework. We assume a single mobile node that needs to be positioned and a set of reference nodes with ideal clocks. In particular, the mobile node's clock is characterized by an affine model described in Section 3.1, node's mobility model is explained in Section 3.2, and the details of the system evolution are laid out in Section 3.3. The application of extended and unscented Kalman filters to the observation is detailed in Section 4. For the sake of reference, Section 4.4 presents the Cramér-Rao bound (derived in Appendix C) for a simplified system model where the mobile node's velocity does not change. Simulation results are discussed in Section 5, where the influence of different parameters is evaluated. Finally, we close the paper with some concluding remarks in Section 6.

2. Related work

Although absolute synchronization is not needed for positioning [37, 38], it might be convenient for other purposes, for example tracking and surveillance, energy conservation in MAC layer protocols, or distributed information processing [32, 39, 40]. There is a vast literature on synchronization in wireless networks. Elson et al. [41], e.g., were among the first to propose a synchronization scheme based on beacons from reference nodes. It must be noted, though, that the interest of the authors was on the synchronization of a wireless network up to a 1 µs and the propagation time of the messages was neglected. Noh, Serpedin and Qarage [42] put forth a synchronization algorithm that accounted for both skew and offset and achieved the Cramér-Rao lower bound. However,

Ref. [42] did not deal with the positioning problem and skew and offset were assumed constant. On the contrary, in this work variation of both characteristics according to a random walk model is assumed. There have been several extensions to the work of Noh and colleagues. For example, Liao and Barooah [43] consider the case of a changing network topology due to the movement of nodes. In our case, we consider a network comprised of a set stationary reference nodes and a single moving node that needs to be positioned, without any changes to the topology, that is, the mobile node is always within the coverage range of the reference nodes. The interested reader may find more information on synchronization in [44–48] and references therein.

One of the earliest works on the joint positioning and synchronization problem is that of Denis, Pierrot and Abou-Rjeily [49]. The authors of this paper proposed a distributed algorithm which converged in several steps. All nodes were assumed stationary and with imperfect clocks, but their characteristics did not change with time. Zheng and Wu [50] considered the problem of a single mobile node and several anchors. Clock inaccuracies of both the mobile node and anchors were considered. However, all nodes were assumed stationary and the clocks drift and offset did not change with time. Refs. [51–58] also considered the situation of unvarying parameters.

Rajan and Van der Veen [59] extended the work in Refs. [51–53] by allowing the wireless nodes to move, but the nodes' positions were not tracked online as all measurements were batch-processed. Yuan et al. [60] allowed the clocks' offset to change according to a random walk model, but they did not consider the clocks' drift. This limitation was lifted by Etzlinger et al. [61] that proposed an algorithm where each node can determine its own varying clock and location parameters in a distributed and sequential manner. The algorithm slices time into equally-long measurement phases. In each measurement phase, nodes exchange time-stamped messages. The message-exchange protocol is asymmetrical in the sense that the number of messages sent from node A to node B may be different than the number of messages from B to A. We follow a divergent approach in this paper and two nodes exchange only two messages in each measurement phase, one in each direction. Moreover, contrary to the situation in Ref. [61], we assume that there is set of perfectly synchronized nodes with known positions. Although this might seem an oversimplification, it appears to be a reasonable assumption in a network with fixed nodes (such as access points in WiFi) and mobile nodes with cheaper clocks.

It must be noted that the problem of joint positioning and synchronization has also been considered in cases where transmission and reception times are not the only observable quantities. For example, Koivisto et al. [62] analyze the problem of DoA/ToA-based (Direction of Arrival/Time of Arrival) positioning and synchronization of user nodes in 5G.

All in all, and to the extent of our knowledge, there is no work in the literature that satisfies all criteria enumerated in Section 1.

3. System model and protocol

3.1. Affine clock model

For the time measured at the mobile node, we assume the commonly used affine model described by [59, 63]

$$= !t + + ; \quad (1)$$

where t is the actual time and is the time as *measured* by the mobile node. The clock drift is modeled by $!$, also known as the clock skew, a dimensionless parameter which is close to unity. The clock offset is represented by and is a measurement noise which we assume zero-mean Gaussian, i.e., $N(0; \ ^2_m)$. Clock skew and offset may vary slowly due to temperature changes and other factors. Although there are more complex clock models [35, 64], we shall adopt a simple discrete random walk model for both parameters.

An idea of the order of magnitude of the parameters in Eq. (1) can be obtained from the literature. For example, Tirado-Andrés and Araujo [36] mention that frequency accuracy of crystal oscillators varies depending on their type, spanning from $0{:}01$ ppm for a MEMs-based oven-controlled crystal oscillator (MEMs OCXO) to $10 \quad 100$ ppm for cheaper quartz crystal oscillators. These values tell us that $j! \quad 1j$ goes from $10^{\ 8}$ to $10^{\ 4}$. Moreover, Tirado-Andrés and Araujo also state that the frequency stability of crystal oscillators is significantly better, between $10^{\ 11}$ and $10^{\ 9}$, when averaged over several seconds or more. These values provide some insight into the slow variation of the skew. An estimate of ^2_m can be found in McElroy, Neirynck and McLaughlin [32], where a variance of the order of $1{:}5 \quad 3 \quad 10^{\ 20}$ s^2 is cited for Ultra Wideband (UWB) commercial products.

As we have already mentioned, we assume that the anchors' clocks are perfectly synchronized and they do not suffer from either drift or offset (a similar assumption is made in, e.g., Ref. [42]). Although this is a strong simplification, it can be lifted without many changes. In spite of the perfect synchronization, we incorporate a zero-mean Gaussian measurement noise with variance ^2_r.

We must note that there is a vast literature on the estimation of the time of arrival of radio signals using super-resolution algorithms such as MUSIC [65–68], ESPRIT [69–74], and SAGE [75–77], among many others [20–23, 78–81]. Since the focus of this work is on tracking a mobile's position and clock, we simply assume that time-of-arrival measurements are subject to a zero-mean normally distributed estimation error.

3.2. Mobility model

For the sake of simplicity, we shall consider that all nodes are located in a two-dimensional space. However, generalization to three dimensions is straightforward. Although anchor nodes are assumed to be stationary, it is simple to extend our results to moving reference nodes with perfectly known positions.

We use the Gauss-Markov Mobility Model [82] for the mobile node. In particular, we assume that its velocity behaves as a random walk with uncorrelated Gaussian steps. This is also known as the random force model [83].

3.3. Details of the system model

Let us slice time into observation periods of length h. At the beginning of the kth observation period (i.e., at $t_k = kh$), $!_k$, $_k$, $[v_k^x; v_k^y]$, and $[x_k^m; y_k^m]$ are the skew, offset, velocity and position of the mobile, respectively. These variables are described by the equations

$$\begin{aligned} !_{k+1} &= !_k + {}_k^!; & {}_{k+1} &= {}_k + {}_k; \\ v_{k+1}^x &= v_k^x + {}_k^{v^x}; & v_{k+1}^y &= v_k^x + {}_k^{v^x}; \\ x_{k+1}^m &= x_k^m + hv_k^x; & y_{k+1}^m &= y_k^m + hv_k^y; \end{aligned}$$

where ${}_k^! \quad N(0; {}_!^2)$, ${}_k \quad N(0; {}^2)$, ${}_k^{v^x}; {}_k^{v^y} \quad N(0; {}_v^2)$ are (transversely and longitudinally) independent. This dynamic model can be written in matrix form as $\mathbf{s}_{k+1} = \mathbf{F}\mathbf{s}_k + \mathbf{G}\tilde{}_k^s$, with

$$\mathbf{s}_k = \begin{pmatrix} !_k \\ {}_k \\ v_k^x \\ v_k^y \\ x_k^m \\ y_k^m \end{pmatrix}; \qquad \mathbf{F} = \begin{pmatrix} 1 & 0 & 0 & 0 & 0 & 0 \\ 0 & 1 & 0 & 0 & 0 & 0 \\ 0 & 0 & 1 & 0 & 0 & 0 \\ 0 & 0 & 0 & 1 & 0 & 0 \\ 0 & 0 & h & 0 & 1 & 0 \\ 0 & 0 & 0 & h & 0 & 1 \end{pmatrix}; \tag{2}$$

$$\tilde{}_k^s = \begin{pmatrix} {}_k^! \\ {}_k \\ {}_k^{v^x} \\ {}_k^{v^y} \end{pmatrix}; \qquad \mathbf{G} = \begin{pmatrix} \mathbf{I}_{4\ 4} \\ \mathbf{0}_{2\ 4} \end{pmatrix}. \tag{3}$$

Alternatively, we may write the system model as $\mathbf{s}_{k+1} = \mathbf{F}\mathbf{s}_k + \tilde{}_k^s$, where $\tilde{}_k^s \ 2 \ \mathbb{R}^6$ is a vector of zero-mean Gaussian random variables with covariance matrix $\mathbf{Q} = \text{diag} \quad {}_!^2; {}^2; {}_v^2; {}_v^2; 0; 0$.

3.4. Protocol and observation model

In principle, our approach is similar to that in many other positioning systems [33, 38, 42]: each anchor node periodically exchanges two messages with the mobile node. Based on these exchanges, the system estimates the position and the velocity of the mobile node as well as the skew and the offset of its clock. This description, however, omits several relevant details.

Since there might be many anchor nodes, a collision of messages from two anchors is possible. Even though this possibility depends on the particularities of the MAC protocol of the communication network, we lean on the fact that reference nodes are perfectly synchronized and propose to order their message exchanges with the mobile node sequentially. Indeed, let us assign each anchor a number from $\{0; 1; \quad ; n \quad 1\}$, where n is the total number of reference nodes. Then, the ith anchor must initiate the message exchange of the kth observation period at $t_k + i \quad$, where $\quad$ is an adequate time interval. On one hand, we need $n \quad < h$, as each reference node must complete its message exchange before the

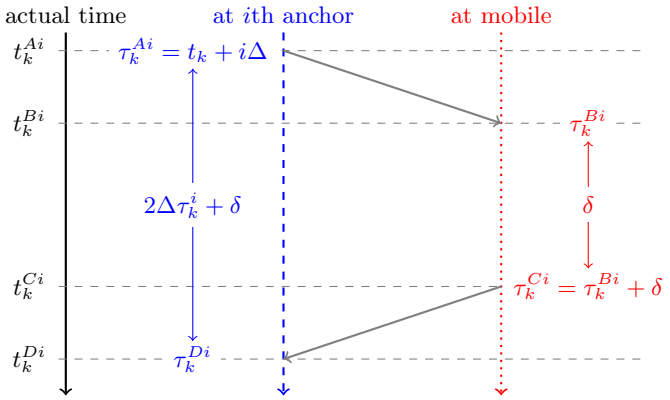

Figure 1: Message exchange between the ith reference node and the mobile node. One message is sent from the reference node to the mobile at time t_k^{Ai} and another one is sent in the reverse direction at time t_k^{Ci}. Actual time (left, black) does not agree with time measured at the ith anchor (center, blue) or time measured at the mobile node (right, red). Estimation algorithms are based on the recorded values of $^{Bi}_{k}$ and $^{i}_{k}$. Time measurement noise is not shown for clarity.

beginning of the following observation period. On the other hand, must be large enough to accommodate a complete round trip time. Neglecting message processing time, the largest acceptable distance from the mobile to the reference nodes is c =2, where c is the speed of light.

Oftentimes, message processing time is neglected in the literature. In this work, we explicitly incorporate this processing time into the protocol. Furthermore, in doing so, we facilitate the estimation of the clock skew as it is explained below. Let us fix an amount of time such that it is larger than the maximum message processing time possible. The protocol commits the mobile to send its reply seconds after the reception of the message from the anchor.

The complete protocol and the resulting observations can be best understood by referring to Fig. 1. We denote actual times with t and *measured* times with the greek letter . We assume that the distance from the mobile to each reference node is constant during each message exchange, but the position of the mobile may change between exchanges with different anchors. In this sense, we implicitly assume that the mobile's speed v is such that v is much smaller than the distance to any anchor, but v can be commensurate with vh. Furthermore, we assume that the mobile velocity, the clock skew and offset vary slowly with time and can be considered constant during the observation period. With all these considerations, the measurement procedure for each anchor node can be described as follows (see Fig. 1):

1. The ith reference node (i = 0; 1; ; n 1) is expected to send a message to the mobile at time $t_k + i$. Let us call $^{Ai}_{k}$ (= $t_k + i$) the sending time measured by the anchor. Although the clock of the ith reference node is perfectly synchronized, various factors (such as the processing load) may

influence the actual sending time.

2. The mobile node records the arrival of the message at time t_k^{Bi}.
3. The mobile sends a message back to the anchor after a pre-defined short time Δ. The message contains the sending time as measured by the mobile node, i.e., $t_k^{Ci} = t_k^{Bi} + \Delta$.
4. The reference node receives this last message at a measured time t_k^{Di}.

After this exchange, the anchor node records two observations:

$$t_k^{Bi}, \qquad z_k^i = \frac{(t_k^{Di} - t_k^{Ai}) - (t_k^{Ci} - t_k^{Bi})}{2}. \tag{4}$$

It can be shown that (see Appendix A for details)

$$\mathsf{E}\left[t_k^{Bi}\right] = \alpha_k(kh + i\Delta) + \alpha_k \frac{d_k^i}{c} + \beta_k, \tag{5}$$

$$\mathsf{E}\left[z_k^i\right] = \frac{d_k^i}{c} + \frac{\Delta}{2}\left(\frac{1}{\alpha_k} - 1\right), \tag{6}$$

and the covariance matrix is given by

$$\mathbf{C}\left[t_k^{Bi}, z_k^i \middle| \mathbf{s}_k\right] = \frac{\sigma_m^2 + \sigma_r^2}{2}\begin{pmatrix} 2 & -1 \\ -1 & 1 \end{pmatrix}. \tag{7}$$

The full vector of observations at the kth period is given by

$$\mathbf{z}_k = \left(t_k^{B0}, z_k^0, t_k^{B1}, z_k^1, \ldots, t_k^{B(n-1)}, z_k^{n-1}\right)^T,$$

where n is the number of anchor nodes. Since the complete system state (see Eq. (2)) has six parameters, at least three anchors (two observations per anchor) are needed.

Equation (6) gives a hint on why the explicit incorporation of the processing time in the protocol eases the estimation of the clock parameters. Indeed, if the protocol had not fixed a *known* value Δ, the second term on the right-hand-side of the equation would include an unknown, probably random, time.

4. Estimation algorithms

There are many estimation algorithms that can deal with a nonlinear observation model as that presented in the previous section, e.g., extended Kalman filters [84–86], unscented Kalman filters [87–90], particle filters [85, 91–93] and unscented particle filters [94]. Although we tried all these alternatives, we found that particle filters exhibited a higher computational cost with no significant improvement in the estimation error. For this reason, in this paper we present results of the extended and unscented Kalman filters.

4.1. Initial Estimation

An initial estimation is needed for both extended and unscented Kalman filters. We use a very simple approach that considers only two observations. We assume that the clock is unskewed, i.e., $\hat{\alpha} = 1$. Offset is estimated as an average

$$\hat{\beta} = \frac{1}{2n} \sum_{k=0}^{} \sum_{i=1}^{} \left({}^{B_i}_{k} - {}^{A_i}_{k} \right) - {}^{i}_{k} \; . \tag{8}$$

Distance to each anchor is estimated assuming the skew is close to unity, that is, $\hat{d}^i_k = c \; {}^{i}_{k}$. The estimation of the mobile's position $(\hat{x}^m_k ; \hat{y}^m_k)$ is obtained through a least-squares fit of the estimated distances. Finally, the mobile's velocity is estimated from a simple incremental quotient

$$\hat{v}^x = \frac{\hat{x}^m_1 - \hat{x}^m_0}{h} ; \qquad \hat{v}^x = \frac{\hat{y}^m_1 - \hat{y}^m_0}{h} . \tag{9}$$

As we show by means of simulations, these rough estimates are sufficient to obtain reasonable results.

4.2. Extended Kalman Filter

The extended Kalman filter (EKF) deals with nonlinearities through a first-order linear approximation around the filter's estimated trajectory. There is a vast literature on the subject (see, e.g., [84, 95] and references therein), so we limit ourselves to present the application of EKF to our problem.

Since the system model is linear (see Section 3.3), we only need to deal with the linearization of the observation. We may write the observation as

$$\mathbf{z} = \mathbf{h} (\mathbf{s}, \boldsymbol{\sim}^z) ; \tag{10}$$

where we have dropped the time subscript for the sake of clarity. $\mathbf{s}$ is the state vector and $\boldsymbol{\sim}^z$ is an observation noise given by

$$\boldsymbol{\sim}^z = \left(\sim^{A1}, \sim^{B1}, \sim^{C1}, \sim^{D1}, \sim^{A2}, \ldots, \sim^{D(n-1)} \right)^T , \tag{11}$$

$$\mathbf{C}_{\boldsymbol{\sim}^z} = \operatorname{diag} \left({}^{2}_{r}, {}^{2}_{m}, {}^{2}_{m}, {}^{2}_{r}, \ldots, {}^{2}_{r} \right) . \tag{12}$$

Eq. (10) can be linearized as

$$\mathbf{z} = \mathbf{z}_0 + \mathbf{H} (\mathbf{s} - \mathbf{s}_0) + \mathbf{W} \boldsymbol{\sim}^z ; \tag{13}$$

where $\mathbf{H}$ and $\mathbf{W}$ are the Jacobians

$$\mathbf{H} = \left. \frac{\partial \mathbf{h}}{\partial \mathbf{s}} \right|_{\mathbf{s}=\mathbf{s}_0 ; \; \boldsymbol{\sim}^z = 0} ; \quad \mathbf{W} = \left. \frac{\partial \mathbf{h}}{\partial \boldsymbol{\sim}^z} \right|_{\mathbf{s}=\mathbf{s}_0 ; \; \boldsymbol{\sim}^z = 0} . \tag{14}$$

These matrices are given by

$$\mathbf{H}_{2i,:} = \begin{pmatrix} 0 & t+i & +\frac{d^i}{c} & 1_T \\ \vdots & & & \\ & 1 & & \\ & !\ {}^{i}i & & \\ & !\ {}^{i}i & & \\ & !\ {}^{i} & & \\ & !\ {}^{i} & & \end{pmatrix} ;\ \mathbf{H}_{2i+1,:} = \begin{pmatrix} 0 & & 1_T \\ & \frac{}{2!^2} & \\ & 0 & \\ & {}^{i}i & \\ & {}^{i}i & \\ & {}^{i} & \\ & {}^{i} & \end{pmatrix} ; \tag{15}$$

$$\mathbf{W}_{2i;4i:4i+3} = \begin{pmatrix} 0 & ! & 1_T \\ & 1 & \\ & 0 & \\ & 0 & \end{pmatrix} ;\ \mathbf{W}_{2i+1;4i:4i+3} = \begin{pmatrix} 0 & & 1_T \\ & \frac{1}{2} & \\ & \frac{1}{2!} & \\ & \frac{1}{2!} & \\ & \frac{1}{2} & \end{pmatrix} ; \tag{16}$$

with t the observation time and

$$^{i} = \frac{x^m + v^x i \quad x^i}{cd^i}; \quad ^{i} = \frac{y^m + v^y i \quad y^i}{cd^i}: \tag{17}$$

We may re-write Eq. (13) as

$$\mathbf{z} = \mathbf{z}_0 + \mathbf{H}(\mathbf{s} \quad \mathbf{s}_0) + ^{\sim z}; \tag{18}$$

where $^{\sim z}\ 2\ \mathsf{R}^{2n}$ is a vector of zero-mean Gaussian random variables with covariance $\mathbf{R} = \mathbf{W}\mathbf{C}_{\sim z}\mathbf{W}^T$.

Finally, at each step k, the extended Kalman filter can be written as shown in Algorithm 1. Observe that we use the Joseph stabilized version of the covariance measurement update equation [86, 95] as we found it more robust in our numerical experiments.

It is interesting to look at the computational cost of the extended Kalman filter in terms of floating point operations. It can be shown that each iteration of the extended Kalman filter takes $O(n^3)$ operations (see Appendix B), where n is the number of anchors. If the mobile node were perfectly synchronized and only one measurement per anchor were taken, a similar extended Kalman filter would require approximately one-eighth the number of operations, but it would still be $O(n^3)$.

4.3. Unscented Kalman Filter

Instead of approximating the nonlinear functions in the dynamic and observation model, the unscented Kalman filter (UKF) approximates the posterior distribution of the parameters given the observation by a Gaussian density represented by a few selected deterministic samples known as sigma points. These sample points allow to compute the true mean and covariance up to a second order of the Taylor expansion of any nonlinear function. Details of the UKF can be found in [87–90] and references therein.

Algorithm 1: Extended Kalman Filter

Prediction step:

$$\hat{\mathbf{s}}_{k|k-1} = \mathbf{F}\hat{\mathbf{s}}_{k-1|k-1};$$
$$\mathbf{P}_{k|k-1} = \mathbf{F}\mathbf{P}_{k-1|k-1}\mathbf{F}^T + \mathbf{Q};$$
$$\hat{\mathbf{z}}_{k|k-1} = h(\hat{\mathbf{s}}_{k|k-1}, \mathbf{0}).$$

Update step:

$$\mathbf{y}_k = \mathbf{z}_k - \hat{\mathbf{z}}_{k|k-1};$$
$$\mathbf{S}_k = \mathbf{H}_k\mathbf{P}_{k|k-1}\mathbf{H}_k^T + \mathbf{R}_k;$$
$$\mathbf{K}_k = \mathbf{P}_{k|k-1}\mathbf{H}_k^T\mathbf{S}_k^{-1};$$
$$\hat{\mathbf{s}}_{k|k} = \hat{\mathbf{s}}_{k|k-1} + \mathbf{K}_k\mathbf{y}_k;$$
$$\mathbf{P}_{k|k} = (\mathbf{I} - \mathbf{K}_k\mathbf{H}_k)\,\mathbf{P}_{k|k-1}\,(\mathbf{I} - \mathbf{K}_k\mathbf{H}_k)^T + \mathbf{H}_k\mathbf{R}_k\mathbf{H}_k^T$$

$\mathbf{R}_k = \mathbf{W}_k\mathbf{C}_{\tilde{z}}\mathbf{W}_k^T$, and $\mathbf{H}_k$ and $\mathbf{W}_k$ are given as in Eqs. (15) and (16), respectively, evaluated at $\mathbf{s} = \hat{\mathbf{s}}_{k|k-1}$

At each step k, the unscented Kalman filter can be written as shown in Algorithm 2 [89]. In those equations, $\lambda = \alpha^2(6 + \kappa) - 6$, where α is a parameter that determines the spread of the sigma points and κ is a secondary scaling value. A guide on how to choose these parameters can be found in the references. In our case, we found that $\alpha = 1$ and $\kappa = 3$ gave good results. Weights W_m^j and W_c^j are calculated as [89]

$$W_m^0 = \frac{\lambda}{6 + \lambda}; \quad W_c^0 = \frac{\lambda}{6 + \lambda} + 1 - \alpha^2 + \beta; \tag{19}$$

$$W_m^j = W_c^j = \frac{1}{2(\alpha^2(6 + \kappa))} \qquad j \neq 0; \tag{20}$$

where β is a parameter which we set equal to two, the optimal value for Gaussian distributions [89].

According to the analysis in Appendix B, each iteration of the unscented Kalman filter requires $O(n^3)$ operations, with n the number of anchors. This result is similar to that of the extended Kalman filter. Indeed, in both cases the more complex computation is the inversion of a matrix of $2n \times 2n$ elements (see the third line of the update step in Algorithm 1 and the fourth line of the update step in Algorithm 2). However, it is easy to see that the unscented Kalman filter requires more operations and this fact is noticeable for small values of n.

Algorithm 2: Unscented Kalman Filter

Calculation of sigma points:

$$\mathbf{D} = \sqrt{(6 + \quad)\mathbf{P}_{k \quad 1jk \quad 1}}^{T};$$

$$S^{0}_{k \quad 1jk \quad 1} = \hat{s}_{k \quad 1jk \quad 1};$$

$$S^{j}_{k \quad 1jk \quad 1} = \hat{s}_{k \quad 1jk \quad 1} + \mathbf{D}_{:;j} \qquad j = 1; \quad ;6;$$

$$S^{j}_{k \quad 1jk \quad 1} = \hat{s}_{k \quad 1jk \quad 1} \quad \mathbf{D}_{:;j} \qquad j = 7; \quad ;12:$$

Prediction step:

$$S^{j}_{kjk \quad 1} = \mathbf{F}S^{j}_{k \quad 1jk \quad 1};$$

$$\hat{s}_{kjk \quad 1} = \sum_{j=0}^{12} W^{j}_{m} S^{j}_{kjk \quad 1};$$

$$S^{j}_{kjk \quad 1} = S^{j}_{kjk \quad 1} \quad \hat{s}_{kjk \quad 1};$$

$$\mathbf{P}_{kjk \quad 1} = \sum_{j=0}^{12} W^{j}_{c} \quad S^{j}_{kjk \quad 1} \quad S^{j}_{kjk \quad 1}{}^{T};$$

$$Z_{kjk \quad 1} = \hbar \quad S^{j}_{kjk \quad 1}; 0 \quad ;$$

$$\hat{z}_{kjk \quad 1} = \sum_{j=0}^{12} W^{j}_{m} Z_{kjk \quad 1}:$$

Update step:

$$Z^{j}_{kjk \quad 1} = Z^{j}_{kjk \quad 1} \quad \hat{z}_{kjk \quad 1};$$

$$\mathbf{P}^{zz}_{k} = \sum_{j=0}^{12} W^{j}_{c} \quad Z^{j}_{kjk \quad 1} \quad Z^{j}_{kjk \quad 1}{}^{T};$$

$$\mathbf{P}^{sz}_{k} = \sum_{j=0}^{12} W^{j}_{c} \quad S^{j}_{kjk \quad 1} \quad Z^{j}_{kjk \quad 1}{}^{T};$$

$$\mathbf{K}_{k} = \mathbf{P}^{sz}_{k} (\mathbf{P}^{zz}_{k})^{\quad 1};$$

$$\hat{s}_{kjk} = \hat{s}_{kjk \quad 1} + \mathbf{K}_{k} \quad z_{k} \quad \hat{z}_{kjk \quad 1} \quad ;$$

$$\mathbf{P}_{kjk} = \mathbf{P}_{kjk \quad 1} \quad \mathbf{K}_{k} (\mathbf{P}^{zz}_{k})^{\quad 1} \mathbf{K}^{T}_{k}:$$

4.4. Cramér-Rao lower bound

It is usually instructive to compare the estimation results to a performance bound such as the Cramér-Rao lower bound (CRB). However, the computation of the CRB in the most general case is too involved. Thus, we only provide an approximation to the CRB in the special case where the mobile speed does not change, i.e., $\sigma_v^2 = 0$. Even with this simplification, the resulting formulas are quite complex and we present them in Appendix C for completeness. In this section, we discuss results for an even simpler scenario that leads to slightly more tractable formulas that may help to gain some intuition.

Let us assume that the mobile's speed is zero ($v_k^x = v_k^y = 0$). Furthermore, let us assume that all reference nodes are randomly distributed on a circumference at a constant distance R from the mobile. For the sake of simplicity, we let $\sigma_m = \sigma_r$. Finally, let us assume that n h and R ch. Under these conditions, it can be shown that the CRB does not depend neither on the distance between the mobile and the reference nodes nor on the parameters and . These conclusions are validated by our simulation results in Section 5. If we further assume that the initial uncertainty is the same for both components of the velocity and for both coordinates of the position, it can be shown that, for large time (large k),

$$\mathrm{CRB}(x^m) = \mathrm{CRB}(y^m) \;/\; \frac{c^2 \sigma_m^2}{kn}; \tag{21}$$

$$\mathrm{CRB}(v^x) = \mathrm{CRB}(v^y) \;/\; \frac{c^2 \sigma_m^2}{h^2 k^3 n}; \tag{22}$$

Thus, the positioning error decreases with time and the number of reference nodes and, for large estimation times, is independent of the time interval h. Clearly, this independence of h is due to the fact that, in this simplified case, the position of the mobile does not change. However, the fact that the positioning error decreases with the number of reference nodes is corroborated by the simulation results.

5. Numerical experiments

In this section, we study the performance of the simultaneous synchronization and localization algorithms under varying conditions. In order to evaluate the influence of the number of reference nodes and the distance between them and the mobile, we set its mean speed to zero and distribute the n reference nodes uniformly (and deterministically) on a circumference of radius R centered at the initial mobile position. The remaining parameters are set as follows:

- We let $q_0 = 1 \quad 10^{-5}$ and $q_1 = 10^{-11}$, both values in accordance to those in the literature (see, e.g., [36]). There is some arbitrariness on the actual value q_0, but we deal with it in other simulations.
- We fix $\sigma_0 = 500$ ns and $\sigma_p = 0{:}01$ ns.

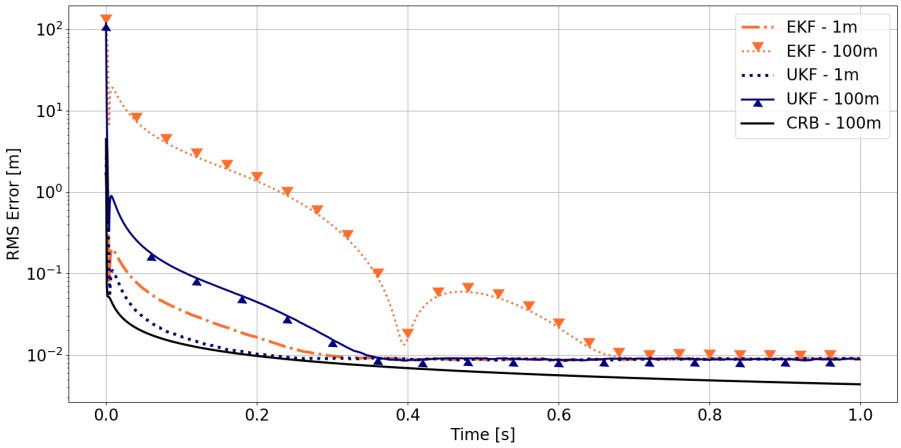

Figure 2: Positioning error vs. time. Performance of UKF (blue) is consistently better than that of EKF (orange). CRB for R = 100 m is shown as a black solid line.

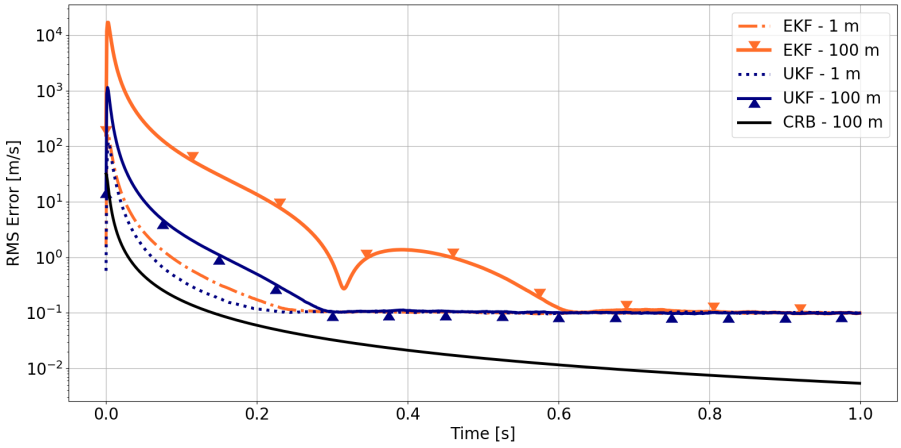

Figure 3: Velocity estimation error vs. time. Performance of UKF (blue) is consistently better than that of EKF (orange).

- $_r$ = $_m$ = 0.2 ns, values commensurate with those reported for commercial products [32].
- For the velocity we arbitrarily set $_v$ = 0.01 m s ^{1}.
- The time intervals are h = 1 ms, = 1 µs and = 5 µs.

Figures 2 and 3 show the root mean square (RMS) positioning and velocity estimation errors, respectively, resulting from the average of 1000 realizations when n = 3. Performance of the unscented Kalman filter is consistently better than that of the extended Kalman filter, but the differences vanish with time.

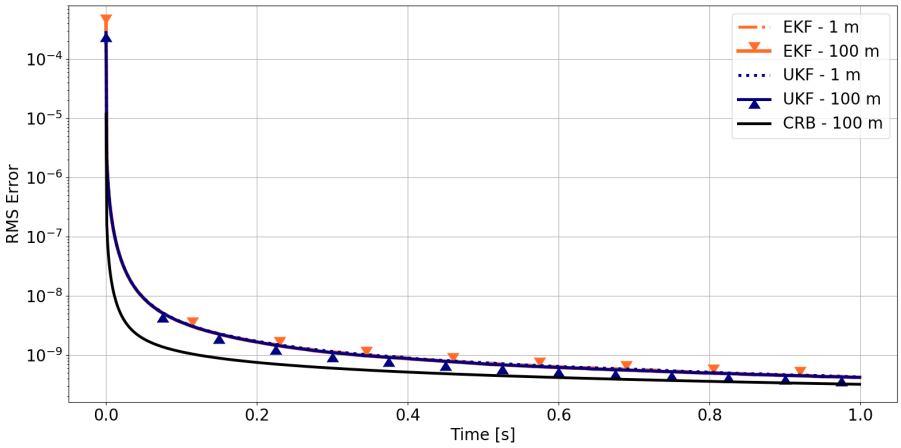

Figure 4: Skew estimation error vs. time. There is no significant difference in performance between UKF (blue) and EKF (orange). Results are independent of the distance to the anchors.

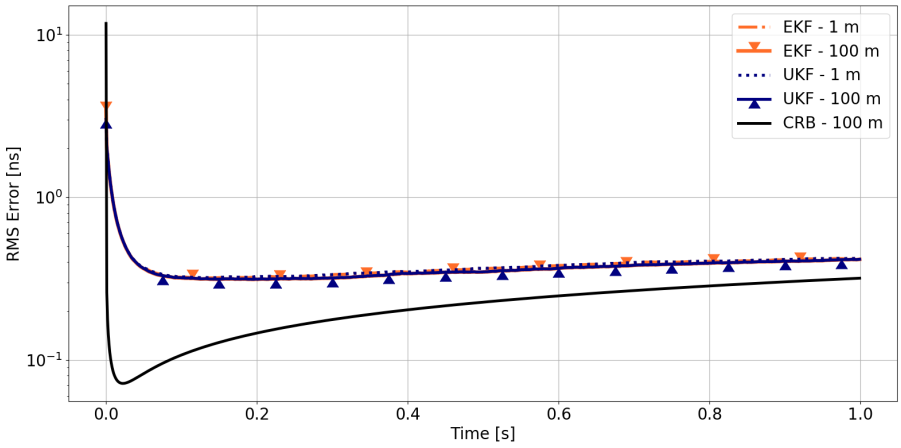

Figure 5: Offset estimation error vs. time. There is no significant difference in performance between UKF (blue) and EKF (orange). Results are independent of the distance to the anchors.

Furthermore, errors are larger for longer distances between the reference nodes and the mobile. However, such difference becomes negligible for longer estimation times. The Cramér-Rao bound continues to decrease with time, while actual errors stabilize close to a minimum. The difference is due to the fact that the CRB was derived under the constant velocity assumption, while in the simulations there are small variations due to $v \neq 0$.

It is interesting to observe that the error of the extended Kalman filter exhibits a non-monotonic behavior in Figs. 2 and 3 when $R = 100$ m. It can be shown that this behavior is present in both algorithms even in the absence

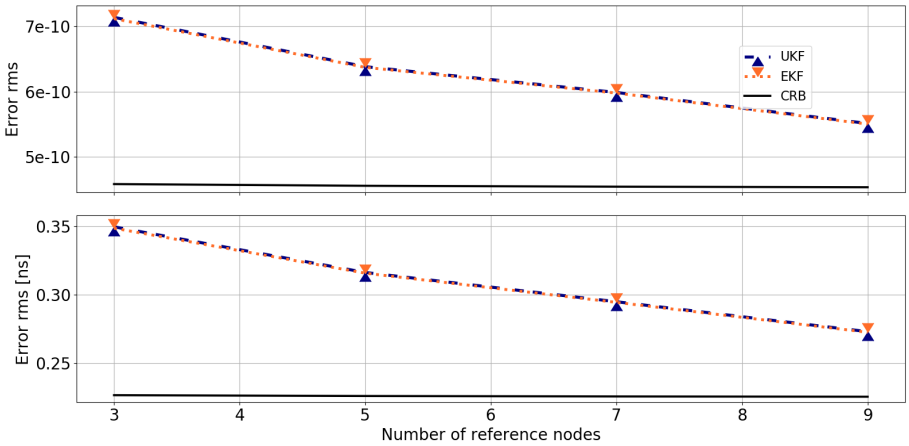

Figure 6: Skew (top) and o□set (bottom) estimation errors after 500 ms vs. number of reference nodes. UKF (blue triangles) and EKF (orange triangles) show similar results. CRB is shown as a black solid line.

of observation noise and with a fixed mobile state. In this sense, the non-monotonic behavior of the error is inherent to the iterative estimation nature of the extended and the unscented Kalman filters under the particular geometry of the problem. Indeed, it can also be shown that if the anchors had been placed in different positions, the details of the behavior of the error would have changed, but not the general trend.

Figures 4 and 5 show the RMS skew and offset estimation errors, respectively. It can be observed that the skew estimation error monotonically decreases with time. In both cases, there is almost no dependence of the error with the distance, a fact predicted by our analysis of the CRB under several simplifying assumptions.

The influence of the number of reference nodes is put in evidence in Figs. 6 and 7, where we show the root mean square errors after 500 ms as a function of the number of reference nodes, for R = 10 m. As it can be observed, there is no significant difference between the extended and the unscented Kalman filter. Moreover, the small difference in performance of both estimators decreases with the number of reference nodes. In all cases, RMS error decreases with the number of nodes, as it might be expected (see discussion in Section 4.4). In Fig. 7, the Cramér-Rao lower bound for the simplified case of constant velocity follows the same decreasing trend as the positioning error.

Performance of the localization and synchronization algorithms do not depend on the offset, as it is evident from Fig. 8 which shows the positioning error after 500 ms for varying values of the mean offset. This result might have been expected as the calculations of the CRB in Appendix C lead to a bound which is independent of the mean offset. It must be noted that, although we do not present them for the sake of brevity, similar results are obtained when the mean skew is varied, that is, errors do not depend significantly on the mean skew, for

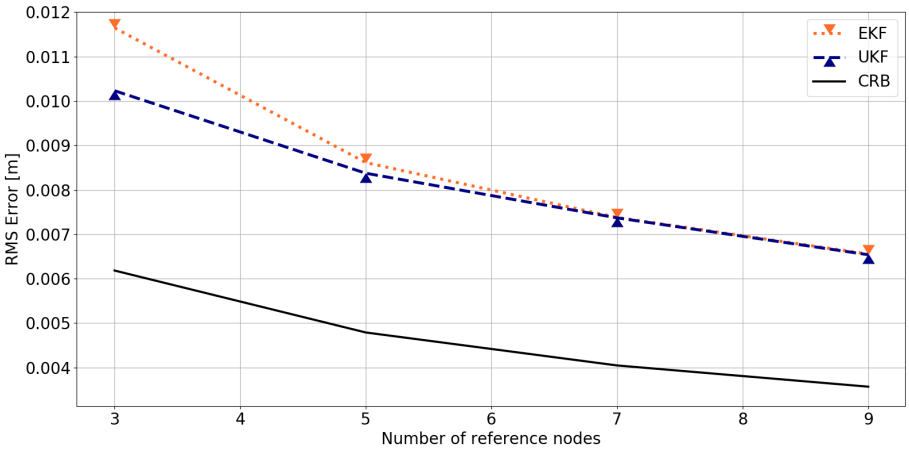

Figure 7: Positioning error after 500 ms vs. number of reference nodes. UKF (blue dashed line) shows slightly better results than EKF (orange pointed line). CRB is shown as a black solid line.

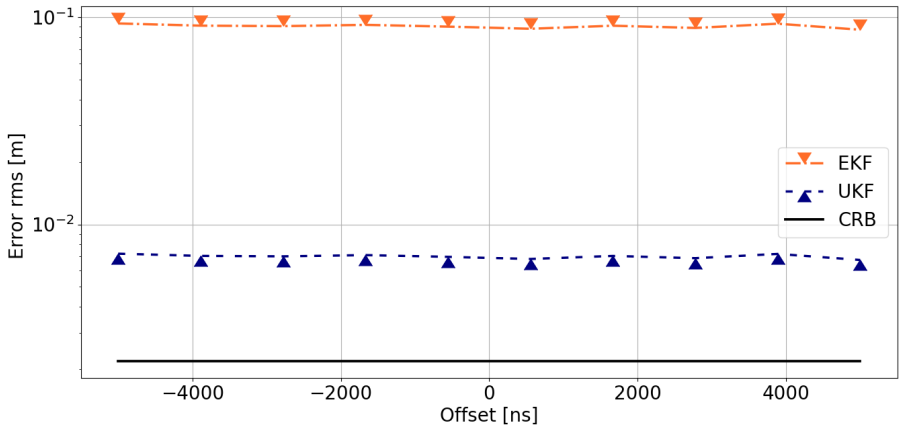

Figure 8: Positioning error vs. mean o□set. Performance of UKF (blue) is consistently better than that of EKF (red). CRB is shown as a black solid line.

reasonable values close to unity.

We study the influence of the mean mobile speed in Fig. 9 which shows the RMS positioning error for two different speeds, 1 ms^{-1} and 10 ms^{-1}. Even though the mean speed is increased by an order of magnitude, the RMS error increases only by a factor of 2.

The case of a perfect clock in the mobile node has been extensively studied in the literature (see Section 2). In this situation, the proposed algorithms continue to work adequately. It is interesting to compare their performance with that of much simpler algorithms that can be used for positioning, although using the same measurements. For example, the position and the velocity can be esti-

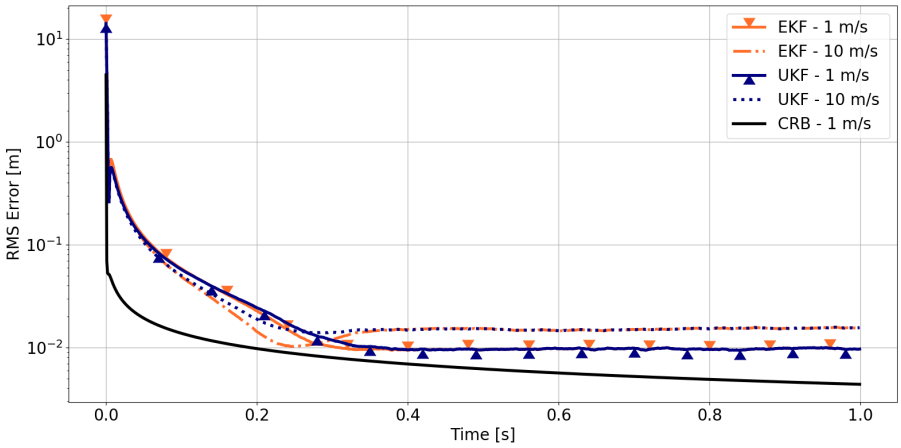

Figure 9: Positioning error vs. time, for different mean speeds of the mobile node. EKF (orange) and UKF (blue) have similar performances. CRB is shown as a black solid line.

mated by fitting the measurements by means of a simple nonlinear least squares optimization algorithm. Figure 10 presents the results for the positioning error when the mobile initial velocity is $v_0^x = v_0^y = 1\,\mathrm{m\,s}^{-1}$ and four reference nodes are used (the remaining parameters are as in, e.g., Fig. 2). The extended and unscented Kalman filters are compared with a least squares algorithm (LSQ). In particular, we use the trust region reflective algorithm, as implemented by the library SciPy of Python, with access to the exact Jacobian of the residuals. As it can be readily seen, after a short 'transient', the least squares algorithm starts to track the mobile node with a small and constant error. However, the RMS error does not improve further and the performance of the LSQ algorithm is ultimately surpassed by that of the EKF and UKF algorithms. All in all, the extended and unscented Kalman filters work well in the case of a perfect clock and their performance is comparable and even better than that of other well-known algorithms.

6. Conclusions

We considered the problem of joint position and clock tracking of a mobile wireless node by a set of reference nodes. Although we assumed the reference nodes to be static, the extension to moving anchors is straightforward. Velocity of the tracked node was assumed to follow a random walk with constant mean. We characterized imperfections of the mobile clock by its skew and offset, both modeled by random walks. In spite that both mobility and clock models can be made more complex, we believe they are sufficient for the application in many real-world positioning systems. We must emphasize that, as we observed in Section 2, many works in the literature assume constant values of the skew, offset or velocity.

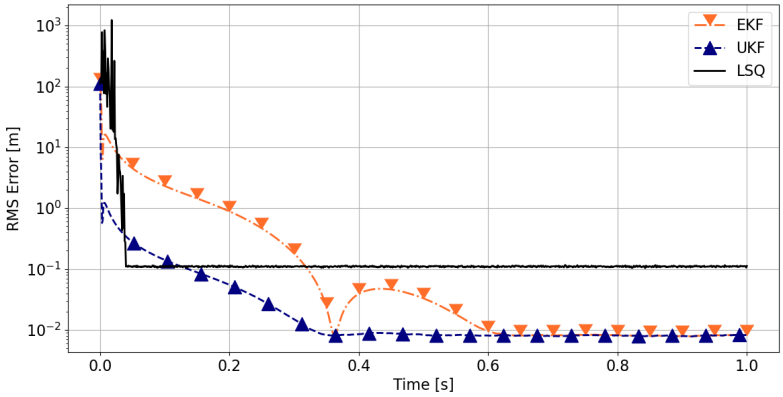

Figure 10: Positioning error (x coordinate) vs. time. While the performances of EKF (orange) and UKF (blue) continue improve, the RMS error of LSQ (black) is constant after a short transient.

We put forth an original measurement protocol similar to that used in two-way ranging. Since two-way ranging protocols are already used in WiFi (see, e.g., [96, 97] and references therein) and commercial UWB products [98], our proposal does not represent an inaccessible engineering feat. However, our proposal differs from a simple two-way ranging protocol in the fact that we accounted explicitly for the message processing time, which is oftentimes neglected in the literature. Given the nonlinearities of the observations, we resorted to the extended and unscented Kalman filters for estimation. We studied the performance of both alternatives by means of extensive simulations, with values of the skew, offset and time measurement noise commensurate with those found in the literature. It must be noted that in these numerical experiments we arbitrarily considered the anchors to be uniformly and deterministically distributed on a circumference. This assumption only simplified our analysis, as a random distribution of reference nodes would have added variation to the results and it would have required a larger number of simulations. All in all, this uniform distribution of anchors enables to easily capture the influence, if any, of the distance between them and the mobile node.

We found that UKF outperforms EKF, although they both produce similar results after a sufficiently long time and for reasonable mobile speeds. Moreover, the distance between the mobile and the anchors appears to be relevant only during an initial acquisition phase of the estimators. We also showed that the mean offset does not affect estimation errors. The influence of mobile speed is minor, although not negligible, with estimation errors increasing with the speed. Finally, we found that positioning errors decrease with the number of anchors.

We also derived the Cramér-Rao bound for a simplified version of the problem that considers a constant velocity. As a consequence, the resulting CRB formulas provide a lower bound, albeit not tight, for the more complex case

considered in the simulations. Moreover, we found that the CRB does not depend on the mean offset, a result which agrees with the observed behavior of the estimation errors.

Since we derived the Cramér-Rao bound in an iterative form, the resulting formulas are quite involved in general. In order to gain some further intuition on the problem, we simplified the analysis by assuming that reference nodes are randomly distributed on a circumference with a static tracked node on its center. This assumption enabled us to average out the dependence of the bound on the actual anchors' positions. We found that positioning errors decrease with the number of anchors and the number of iterations, and increase with time measurement errors. More importantly, positioning errors are largely independent of the distance between the anchors and the tracked node, as observed in the simulation results.

As it was stated in Section 3.2, the proposed algorithms can be straightforwardly extended to deal with the positioning problem in three dimensions. Indeed, the 3D problem requires the addition of two new components to the state vector in Eq. (2) and the modification of just a few equations and definitions. Nonetheless, it must be noted that these modifications imply a slight increase in the numerical complexity of the algorithms. Moreover, the minimum number of anchor nodes required for complete mobile positioning and clock tracking increases from three to four.

A subject of future work is the combination of time-of-arrival estimations with direction-of-arrival (DoA) and angle-of-arrival (AoA) measurements, as it is done in Ref. [62]. This is a most relevant problem as, for example, many WiFi products include more than one antenna and MIMO systems enable AoA estimation. Moreover, massive-MIMO systems in 5G networks appear to be capable of accurate AoA measurements [99].

Acknowledgment

This work was funded by the project PID 2015 # 3 from the Agencia Nacional de Promoción de la Investigación, el Desarrollo Tecnológico y la Innovación (ANPCyT), Argentina.

Appendix A. Details of the observation model

We assume that there is not a significant change of the position of the mobile during the message exchange with a given reference node. This implies, for the kth measurement period of the ith reference node, that

$$k\forall_k k \quad \frac{2d_k^i}{c} + \qquad d_k^i;$$

where $\forall_k$ is the mobile velocity, c the speed of light and d_k^i the distance between the mobile node and the ith anchor at the kth observation time. If we assume

that $k\forall_k k\, d_k^i = c$ (as expected from mobile speeds much smaller than c), then

$$k\forall_k k \quad d_k^i.$$

For example, if = 1 µs and $k\forall_k k$ = 100 m=s (= 360 km=h), then distance it is required d_k^i 0:1 mm.

Based on the quasi-static assumption, in the following calculations we shall fix the distance between the mobile node and the ith reference node at the kth observation time to

$$d_k^i = \sqrt{(x_k^m + v_k^x i \quad x^i)^2 + (y_k^m + v_k^y i \quad y^i)^2}; \tag{A.1}$$

where x^i and y^i are the (fixed) coordinates of the anchor node. We must note that there is another assumption implicit in this equation. Indeed, the actual message exchange is expected to start at a time $kh + i$, but it starts at a slightly different time due to small timing errors in the ith anchor node. We have neglected this small time difference in the calculation of d_k^i because we expect $_r$, where $_r$ is the standard deviation of the reference node's timing errors. This approximation allows us to consider d_k^i is a deterministic value given the state s_k.

Figure 1 shows the message exchange between the ith anchor and the mobile schematically. It must be noted, though, that Fig. 1 does not include timing noise errors for simplicity. Although the ith reference node is perfectly synchronized, various factors (such as the processing load) may influence the actual message sending time of the first message in the exchange:

$$t_k^{Ai} = {}_k^{Ai} \quad {}_k^{Ai} = kh + i \quad {}_k^{Ai}; \tag{A.2}$$

where ${}_k^{Ai}$ $N(0; {}_r^2)$ is a random variable independent of all the variables in the model. The fact that we subtract ${}_k^i$ is conventional (so = t +) and it does not affect the calculations. This message is received by the mobile node at (see Fig. 1)

$$t_k^{Bi} = t_k^{Ai} + \frac{d_k^i}{c}. \tag{A.3}$$

The time recorded by the mobile node is

$${}_k^{Bi} = !_k t_k^{Bi} + {}_k + {}_k^{Bi} \tag{A.4}$$

$$= !_k {}_k^{Ai} + !_k \frac{d_k^i}{c} + {}_k \quad !_k {}_k^{Ai} + {}_k^{Bi}; \tag{A.5}$$

where ${}_k^{Bi}$ $N(0; {}_m^2)$ is an independent random variable.

The mobile node sends a message back to the anchor at a *measured* time ${}_k^{Ci} = {}_k^{Bi} +$. This measured time corresponds to an actual time t_k^{Ci} which satisfies (see Fig. 1)

$${}_k^{Ci} = {}_k^{Bi} + = !_k t_k^{Ci} + {}_k + {}_k^{Ci}) \tag{A.6}$$

$$t_k^{Ci} = \frac{{}_k^{Bi} + \quad {}_k \quad {}_k^{Ci}}{!_k}; \tag{A.7}$$

where $\epsilon_k^{Ci} \sim N(0; \sigma_m^2)$ is an independent random variable. Using Eq. (A.5), we obtain

$$t_k^{Ci} = t_k^{Ai} + \frac{d_k^i}{c} + \frac{1}{\beta_k}\left(t_k^{Ai} + \frac{t_k^{Bi} - t_k^{Ci}}{\beta_k}\right). \tag{A.8}$$

The second message arrives at the ith reference node at

$$t_k^{Di} = t_k^{Ci} + \frac{d_k^i}{c}. \tag{A.9}$$

The measured arrival time is $t_k^{Di} = t_k^{Di} + \epsilon_k^{Di}$, where $\epsilon_k^{Di} \sim N(0; \sigma_r^2)$ is an independent random variable. Thus,

$$t_k^{Di} = t_k^{Ai} + 2\frac{d_k^i}{c} + \frac{1}{\beta_k}\left(t_k^{Ai} + \frac{t_k^{Bi} - t_k^{Ci}}{\beta_k}\right) + \epsilon_k^{Di}. \tag{A.10}$$

Finally, the observation variable is given by

$$\delta_k^i = \frac{(t_k^{Di} - t_k^{Ai}) - (t_k^{Ci} - t_k^{Bi})}{2} \tag{A.11}$$

$$= \frac{d_k^i}{c} + \frac{1}{2}\left(\frac{1}{\beta_k} - 1\right) + \frac{t_k^{Di} - t_k^{Ai}}{2} + \frac{t_k^{Bi} - t_k^{Ci}}{2\beta_k}. \tag{A.12}$$

Based on Eqs. (A.5) and (A.12), we get

$$\mathrm{E}\left[t_k^{Bi} \mid s_k\right] = \beta_k(kh + i - 1) + \beta_k\frac{d_k^i}{c} + \alpha_k, \tag{A.13}$$

$$\mathrm{E}\left[\delta_k^i \mid s_k\right] = \frac{d_k^i}{c} + \frac{1}{2}\left(\frac{1}{\beta_k} - 1\right), \tag{A.14}$$

$$\mathrm{Var}\left[t_k^{Bi} \mid s_k\right] = (\beta_k)^2\sigma_r^2 + \sigma_m^2, \tag{A.15}$$

$$\mathrm{Var}\left[\delta_k^i \mid s_k\right] = \frac{\sigma_m^2}{2(\beta_k)^2} + \frac{\sigma_r^2}{2}, \tag{A.16}$$

$$\mathrm{Cov}\left[t_k^{Bi}, \delta_k^i \mid s_k\right] = \frac{\sigma_m^2}{2\beta_k} + \frac{\beta_k\sigma_r^2}{2}. \tag{A.17}$$

Since we assume that $|\beta_k| \approx 1$, the covariance matrix is approximately constant:

$$\mathbf{C}\left[t_k^{Bi}, \delta_k^i \mid s_k\right] \approx \frac{\sigma_m^2 + \sigma_r^2}{2}\begin{pmatrix} 2 & 1 \\ 1 & 1 \end{pmatrix}. \tag{A.18}$$

Appendix B. Computational cost

Let us analyze the cost of each line in Algorithm 1:

- Prediction step:

- First two lines: it is simple to show that they take $O(1)$ operations.
- Third line: from the discussion in Appendix A, it is easy to show that it takes $O(n)$ operations, where n is the number of nodes.

- Update step: Computation of matrix $\mathbf{H}_k$ takes $O(n)$ operations. The structure of matrices $\mathbf{W}_k$ and $\mathbf{C}_{\sim z}$ implies that the computation of $\mathbf{R}_k$ can be done with $O(1)$ operations.
  - First line: it takes $O(n)$ operations.
  - Second line: due to the matrix products, it takes $O(n^2)$ operations.
  - Third line: matrix products take $O(n^2)$ operations. A naive implementation of the inverse of $\mathbf{S}_k$ takes $O(n^3)$ operations. Although there are more efficient algorithms for the calculation of the inverse of a matrix, in practice, for the sake of an improved numerical stability, we calculate the Moore-Penrose pseudo-inverse of $\mathbf{S}_k$. The computation of the pseudo-inverse takes $O(n^3)$ operations [100].
  - Fourth line: it is simple to show that it takes $O(n)$ operations.
  - Fifth line: due to the structure of $\mathbf{R}_k$, it can be shown that it takes $O(n)$ operations.

Summarizing, each iteration of the extended Kalman filter takes $O(n^3)$ operations.

Let us now focus on the computational cost of the Algorithm 2:

- Calculation of sigma points: since the length of the state vector is fixed, it is simple to see that $O(1)$ operations are required.
- Prediction step: values W_m^j can be computed before starting the iterations.
  - First four lines: again, since the length of the state vector is fixed, these lines can be computed using $O(1)$ operations.
  - Fifth line: as in the third line of Algorithm 1, it can be computed using $O(n)$ operations.
  - Sixth line: by a similar reasoning, $O(n)$ operations are required.
- Update step:
  - First line: it is simple to see that it requires $O(n)$ operations.
  - Second line: since $\mathcal{Z}^j_{kjk\ 1} \in \mathbb{R}^{2n\ 1}$, the matrix product in each term of the right-hand-side requires $4n^2$ operations. Thus, the second line can be computed using $O(n^2)$ operations.
  - Third line: since $\mathcal{S}^j_{kjk\ 1} \in \mathbb{R}^{n\ 1}$, it is easy to show that it requires $O(n)$ operations.

- Fourth line: the product of $\mathbf{P}_k^{sz} \in \mathbb{R}^{6 \times 2n}$ and $(\mathbf{P}_k^{zz})^{-1} \in \mathbb{R}^{2n \times 2n}$ can be done with $O(n^2)$ operations. As in the case of $\mathbf{S}_k$ in the extended Kalman filter, in practice we compute the pseudo-inverse of $\mathbf{P}_k^{zz}$, requiring $O(n^3)$ operations.
- Fifth line: it is simple to see that it requires $O(n)$ operations.
- Sixth line: the product in the second term requires $O(n^2)$ operations.

All in all, each iteration of the unscented Kalman filter requires $O(n^3)$ operations.

For the sake of comparison, let us consider the problem of tracking the mobile position and velocity in the case of a perfectly synchronized mobile clock. In this case, it is evident that each anchor needs to exchange only one message with the mobile node. Both, the extended Kalman filter and the unscented Kalman filter can be used in this case. Although we do not develop all the corresponding equations, it is clear that the main difference in the computational cost is in the third line of the update step of Algorithm 1 and the fourth line of the update step of Algorithm 2. Since there are now only n measurements, matrices $\mathbf{S}_k, \mathbf{P}_k^{zz} \in \mathbb{R}^{n \times n}$. This implies that, roughly, the computation complexity of both algorithms is reduced to $1/8$ that of the corresponding algorithms in the unsynchronized case.

Appendix C. Details of the Cramér-Rao lower bound

Our calculation of the Cramér-Rao bound is based on the recursive computation of the information matrix presented by Tichavsky et al. [101]. The Cramér-Rao bound can be written as (see [85, 101])

$$\mathbf{P}_{kjk} \dot{\geq} \mathrm{E}\left[\left(\hat{\mathbf{s}}_{kjk} - \mathbf{s}_k\right)\left(\hat{\mathbf{s}}_{kjk} - \mathbf{s}_k\right)^T\right] \geq \mathbf{J}_k^{-1}; \tag{C.1}$$

where the inequality means that $\mathbf{P}_{kjk} - \mathbf{J}_k^{-1}$ is a positive semidefinite matrix. Let us introduce $\mathbf{S}_k$, the information matrix of $(\mathbf{r}_{k-1}, \mathbf{v}_{k-1}, \mathbf{s}_k^T)^T$. It can be shown that $\mathbf{J}_k$ and $\mathbf{S}_k$ satisfy the following recurrence equations (see Proposition 2 in Ref. [101])

$$\begin{aligned}
\mathbf{S}_{k+1} &= \begin{pmatrix} \mathbf{S}_{k+1}^{11} & \mathbf{S}_{k+1}^{12} & \mathbf{S}_{k+1}^{13} \\ \mathbf{S}_{k+1}^{21} & \mathbf{S}_{k+1}^{22} & \mathbf{S}_{k+1}^{23} \\ \mathbf{S}_{k+1}^{31} & \mathbf{S}_{k+1}^{32} & \mathbf{S}_{k+1}^{33} \end{pmatrix} \\
&= \mathbf{M}^{-T} \begin{pmatrix} \mathbf{J}_k^{11} + \mathbf{H}_k^{11} & \mathbf{J}_k^{12} + \mathbf{H}_k^{12} & \mathbf{H}_k^{13} \\ \left(\mathbf{J}_k^{12} + \mathbf{H}_k^{12}\right)^T & \mathbf{J}_k^{22} + \mathbf{H}_k^{22} & \mathbf{H}_k^{23} \\ \left(\mathbf{H}_k^{13}\right)^T & \left(\mathbf{H}_k^{23}\right)^T & \mathbf{H}_k^{33} \end{pmatrix} \mathbf{M}^{-1};
\end{aligned} \tag{C.2}$$

$$\begin{aligned}
\mathbf{J}_{k+1} &= \begin{pmatrix} \mathbf{S}_{k+1}^{22} & \mathbf{S}_{k+1}^{23} \\ \mathbf{S}_{k+1}^{32} & \mathbf{S}_{k+1}^{33} \end{pmatrix} - \begin{pmatrix} \mathbf{S}_{k+1}^{21} \\ \mathbf{S}_{k+1}^{31} \end{pmatrix} \left(\mathbf{S}_{k+1}^{11}\right)^{-1} \left(\mathbf{S}_{k+1}^{12}, \mathbf{S}_{k+1}^{13}\right); \\
\mathbf{J}_k &= \begin{pmatrix} \mathbf{J}_k^{11} & \mathbf{J}_k^{12} \\ \mathbf{J}_k^{21} & \mathbf{J}_k^{22} \end{pmatrix}.
\end{aligned} \tag{C.3}$$

We simplify the resulting formulas in two ways. First, we assume that the velocity does not change, i.e., $\sigma_v^2 = 0$. Second, we assume that the distribution of ω_k is narrow and $\omega_k \approx 1$ is a reasonable approximation in all expectations with respect to this random variable. This is an adequate assumption for real-world values of the skew. Under this setting, it can be shown that

$$\mathbf{M} = \begin{pmatrix} 1 & 0 & 0 & 0 & 0 & 0 & 0 & 0 \\ 0 & 1 & 0 & 0 & 0 & 0 & 0 & 0 \\ 0 & 0 & 0 & 0 & 0 & 0 & 1 & 0 \\ 0 & 0 & 0 & 0 & 0 & 0 & 0 & 1 \\ 0 & 0 & 1 & 0 & 0 & 0 & 0 & 0 \\ 0 & 0 & 0 & 1 & 0 & 0 & 0 & 0 \\ 0 & 0 & h & 0 & 1 & 0 & 0 & 0 \\ 0 & 0 & 0 & h & 0 & 1 & 0 & 0 \end{pmatrix}; \tag{C.4}$$

$$\mathbf{H}_k^{11} = \begin{pmatrix} \omega^2 & 0 \\ 0 & \end{pmatrix}_2; \quad \mathbf{H}_k^{12} = \mathbf{0}; \quad \mathbf{H}_k^{13} = \mathbf{H}_k^{11}; \tag{C.5}$$

$$\mathbf{H}_k^{22} = \frac{2}{c(\sigma_m^2 + \sigma_r^2)} \sum_{i=0}^{n-1} \frac{1}{(d_{k+1}^i)^2} \begin{pmatrix} a_k & b_k & c_k & d_k \\ b_k & e_k & d_k & f_k \\ c_k & d_k & g_k & h_k \\ d_k & f_k & h_k & i_k \end{pmatrix}; \tag{C.6}$$

$$\mathbf{H}_k^{23} = \frac{}{c(\sigma_m^2 + \sigma_r^2)} \sum_{i=0}^{n-1} \frac{1}{d_{k+1}^i} \begin{pmatrix} j_k & 0 \\ l_k & 0 \\ m_k & 0 \\ p_k & 0 \end{pmatrix}; \tag{C.7}$$

$$\mathbf{H}_k^{33} = \mathbf{H}_k^{11} + \frac{1}{\sigma_m^2 + \sigma_r^2} \begin{pmatrix} r_k & q_k \\ q_k & 2 \end{pmatrix}; \tag{C.8}$$

where we have defined

$$\begin{aligned}
a_k &= (x_{k+1}^i)^2 (h + i\omega)^2; & b_k &= x_{k+1}^i y_{k+1}^i (h + i\omega)^2; \\
c_k &= (x_{k+1}^i)^2 (h + i\omega); & d_k &= x_{k+1}^i y_{k+1}^i (h + i\omega); \\
e_k &= (y_{k+1}^i)^2 (h + i\omega)^2; & f_k &= (x_{k+1}^i)^2 (h + i\omega); \\
g_k &= (x_{k+1}^i)^2; & h_k &= x_{k+1}^i y_{k+1}^i; \\
i_k &= (y_{k+1}^i)^2; & j_k &= x_{k+1}^i (h + i\omega); \\
l_k &= y_{k+1}^i (h + i\omega); & m_k &= x_{k+1}^i; \\
p_k &= y_{k+1}^i; & q_k &= 2\left(kh + i\omega + \frac{d_{k+1}^i}{c} + \frac{}{2}\right);
\end{aligned}$$

$$r_k = 4 + 6\,\frac{2}{r} + 2\,\frac{2}{m}\,\frac{2}{r}\,\frac{\frac{2}{m}}{\frac{2}{m}+\frac{2}{r}}\left(\frac{d^i_{k+1}}{c}\right)^2 + 2\,(kh+i\,)\,\frac{d^i_{k+1}}{c} + 2\,(kh+i\,)\,\frac{d^i_{k+1}}{c} + {}^2\,\frac{2}{m}+\frac{2}{r}\,{}^2;$$

$$x^i_{k+1} = x^m_k + v^x_k(h+i\,) \quad x^i;$$
$$y^i_{k+1} = y^m_k + v^y_k(h+i\,) \quad y^i$$
$$d^2_{k+1} = \sqrt{x^i_{k+1}{}^2 + y^i_{k+1}{}^2}:$$

For the sake of simplicity, let us assume independent Gaussian priors: $!_0 \sim N(1;\ \frac{2}{w})$, $_0 \sim N(0;\ \frac{2}{p})$, $v^x \sim N(v^x;\ \frac{2}{v^x})$, $v^y \sim N(v^y;\ \frac{2}{v^y})$, $x^m_0 \sim N(x^m_0;\ \frac{2}{x})$. $y^m_0 \sim N(y^m_0;\ \frac{2}{y})$. Then, we may write

$$\mathbf{J}_0{}^{1} = \mathrm{diag}\left[\frac{2}{w};\ \frac{2}{p};\ \frac{2}{v^x};\ \frac{2}{v^y};\ \frac{2}{x};\ \frac{2}{y}\right] \tag{C.9}$$
$$\mathbf{S}_0{}^{1} = \mathrm{diag}\left[\frac{2}{w};\ \frac{2}{p};\ \frac{2}{w};\ \frac{2}{p};\ \frac{2}{v^x};\ \frac{2}{v^y};\ \frac{2}{x};\ \frac{2}{y}\right]: \tag{C.10}$$

It can be instructive to analyze the Cramér-Rao lower bound in a simplified scenario. Let us assume that the mobile's speed is zero ($v^x_k = v^y_k = 0$). Furthermore, let us assume that all references nodes are randomly distributed on a circumference at a constant distance R from the mobile. The previous equations are greatly simplified by taking expectations with respect to these random positions. For the sake of simplicity, we let $_m = {}_r$. Finally, let us assume that n h and R ch. Under these conditions, it can be shown that

$$\mathbf{H}^{23}_k = \mathbf{0}; \tag{C.11}$$
$$\mathbf{H}^{22}_k \quad \frac{n}{2c^2\,\frac{2}{m}}\begin{pmatrix} h^2 & 0 & h & 0 \\ 0 & h^2 & 0 & h \\ h & 0 & 1 & 0 \\ 0 & h & 0 & 1 \end{pmatrix}; \tag{C.12}$$
$$\mathbf{H}^{33}_k \quad \frac{n}{\frac{2}{m}}\begin{pmatrix} (kh)^2 + \frac{\frac{2}{m}}{n\ \frac{2}{l}} & kh \\ kh & 1 + \frac{\frac{2}{m}}{n^{\frac{2}{2}}} \end{pmatrix}: \tag{C.13}$$

After some lengthy calculations, it can be shown that

$$\mathbf{J}_k = \begin{pmatrix} j_{11} & j_{12} & 0 & 0 & 0 & 0 \\ j_{12} & j_{22} & 0 & 0 & 0 & 0 \\ 0 & 0 & j_{33} & 0 & j_{35} & 0 \\ 0 & 0 & 0 & j_{44} & 0 & j_{46} \\ 0 & 0 & j_{35} & 0 & j_{55} & 0 \\ 0 & 0 & 0 & j_{46} & 0 & j_{66} \end{pmatrix}; \tag{C.14}$$

$$j_{33} = {}^{2}_{v^x} + k^2h^2\ {}^{2}_{x} + \frac{2k^3 + 3^2 \quad 5k}{12}\frac{nh^2}{c^2\ {}^{2}_{m}}; \tag{C.15}$$

$$j_{44} = {}^{2}_{vy} + k^2h^2\ {}^{2}_{y} + \frac{2k^3 + 3^2 \quad 5k}{12}\frac{nh^2}{c^2\ {}^{2}_{m}}; \tag{C.16}$$

$$j_{35} = \quad kh\ {}^{2}_{x} \quad \frac{hk(k+1)n}{4c^2\ {}^{2}_{m}}; \tag{C.17}$$

$$j_{46} = \quad kh\ {}^{2}_{x} \quad \frac{hk(k+1)n}{4c^2\ {}^{2}_{m}}; \tag{C.18}$$

$$j_{55} = {}^{2}_{x} + \frac{kn}{2c^2\ {}^{2}_{m}}; \tag{C.19}$$

$$j_{66} = {}^{2}_{y} + \frac{kn}{2c^2\ {}^{2}_{m}}; \tag{C.20}$$

where we have not written down expressions for j_{11}, j_{12} and j_{22} as they are too complex and do not help to provide any intuition.

References

[1] A. Bensky, Wireless positioning technologies and applications, Artech House, 2008.

[2] H. Elayan, R. Shubair, Robust Algorithms for Localizing Moving Nodes in Wireless Sensor Networks, arXiv preprint (2018). arXiv:1806.11214.

[3] S. Li, M. Hedley, K. Bengston, D. Humphrey, M. Johnson, W. Ni, Passive Localization of Standard WiFi Devices, IEEE Systems Journal 13 (4) (2019) 3929–3932.

[4] D. Dardari, M. Luise, E. Falletti, Satellite and terrestrial radio positioning techniques: a signal processing perspective, Academic Press, 2012.

[5] H. Liu, H. Darabi, P. Banerjee, J. Liu, Survey of wireless indoor positioning techniques and systems, IEEE Transactions on Systems, Man, and Cybernetics, Part C (Applications and Reviews) 37 (6) (2007) 1067–1080.

[6] Y. Gu, A. Lo, I. Niemegeers, A survey of indoor positioning systems for wireless personal networks, IEEE Communications Surveys and Tutorials 11 (1) (2009) 13–32.

[7] H. Koyuncu, S. H. Yang, A survey of indoor positioning and object locating systems, IJCSNS International Journal of Computer Science and Network Security 10 (5) (2010) 121–128.

[8] K. Al Nuaimi, H. Kamel, A survey of indoor positioning systems and algorithms, in: 2011 International Conference on Innovations in Information Technology, 2011, pp. 185–190.

[9] T. J. Chowdhury, C. Elkin, V. Devabhaktuni, D. B. Rawat, J. Oluoch, Advances on localization techniques for wireless sensor networks: A survey, Computer Networks 110 (2016) 284–305.

[10] J. P. Grisales Campeón, S. López, S. R. de Jesús Meleán, H. Moldovan, D. R. Parisi, P. I. Fierens, Indoor positioning based on rssi of wifi signals: how accurate can it be?, in: 2018 IEEE Biennial Congress of Argentina (ARGENCON), 2018, pp. 1–8.

[11] J. P. Grisales Campeón, S. López, S. R. de Jesús Meleán, H. Moldovan, D. R. Parisi, P. I. Fierens, Fusion of magnetic and WiFi fingerprints for indoor positioning, in: 2018 Congreso Argentino de Ciencias de la Informática y Desarrollos de Investigación (CACIDI), 2018, pp. 1–5.

[12] J. Yang, Y. Chen, Indoor localization using improved RSS-based lateration methods, in: GLOBECOM 2009 - 2009 IEEE Global Telecommunications Conference, 2009, pp. 1–6.

[13] F. Zafari, A. Gkelias, K. K. Leung, A Survey of Indoor Localization Systems and Technologies, IEEE Communications Surveys and Tutorials 21 (3) (2019) 2568–2599.

[14] Z. Sahinoglu, S. Gezici, I. Güvenc, Ultra-wideband Positioning Systems: Theoretical Limits, Ranging Algorithms, and Protocols, Cambridge University Press, 2008.

[15] A. Makki, A. Siddig, M. Saad, C. Bleakley, Survey of WiFi positioning using time-based techniques, Computer Networks 88 (2015) 218–233.

[16] R. Yamasaki, A. Ogino, T. Tamaki, T. Uta, N. Matsuzawa, T. Kato, TDOA location system for IEEE 802.11b WLAN, in: IEEE Wireless Communications and Networking Conference, 2005, Vol. 4, 2005, pp. 2338–2343.

[17] J. Figueiras, S. Frattasi, Mobile Positioning and Tracking: From Conventional to Cooperative Techniques, John Wiley & Sons, 2010.

[18] A. Mallat, J. Louveaux, L. Vandendorpe, UWB based positioning in multipath channels: CRBs for AOA and for hybrid TOA-AOA based methods, in: 2007 IEEE International Conference on Communications, 2007, pp. 5775–5780.

[19] N. A. Alsindi, B. Alavi, K. Pahlavan, Measurement and modeling of ultrawideband TOA-based ranging in indoor multipath environments, IEEE Transactions on Vehicular Technology 58 (3) (2008) 1046–1058.

[20] D. Dardari, A. Conti, U. Ferner, A. Giorgetti, M. Z. Win, Ranging with ultrawide bandwidth signals in multipath environments, Proceedings of the IEEE 97 (2) (2009) 404–426.

[21] W. Xu, M. Huang, C. Zhu, A. Dammann, Maximum likelihood TOA and OTDOA estimation with first arriving path detection for 3GPP LTE system, Transactions on Emerging Telecommunications Technologies 27 (3) (2016) 339–356.

[22] Z. Sahinoglu, I. Guvenc, Multiuser interference mitigation in noncoherent UWB ranging via nonlinear filtering, EURASIP Journal on Wireless Communications and Networking 2006 (1) (2006) 056849.

[23] D. Dardari, A. Giorgetti, M. Z. Win, Time-of-arrival estimation of UWB signals in the presence of narrowband and wideband interference, in: 2007 IEEE International Conference on Ultra-Wideband, 2007, pp. 71–76.

[24] P.-C. Chen, A non-line-of-sight error mitigation algorithm in location estimation, in: WCNC. 1999 IEEE Wireless Communications and Networking Conference (Cat. No. 99TH8466), Vol. 1, 1999, pp. 316–320.

[25] X. Wang, Z. Wang, B. O'Dea, A TOA-based location algorithm reducing the errors due to non-line-of-sight (NLOS) propagation, IEEE Transactions on Vehicular Technology 52 (1) (2003) 112–116.

[26] L. Cong, W. Zhuang, Nonline-of-sight error mitigation in mobile location, IEEE Transactions on Wireless Communications 4 (2) (2005) 560–573.

[27] I. Guvenc, C.-C. Chong, F. Watanabe, NLOS identification and mitigation for UWB localization systems, in: 2007 IEEE Wireless Communications and Networking Conference, 2007, pp. 1571–1576.

[28] S. Marano, W. M. Gifford, H. Wymeersch, M. Z. Win, NLOS identification and mitigation for localization based on UWB experimental data, IEEE Journal on Selected Areas in Communications 28 (7) (2010) 1026–1035.

[29] Y. Shimizu, Y. Sanada, Accuracy of relative distance measurement with ultra wideband system, Electronics and Communications in Japan (Part III: Fundamental Electronic Science) 87 (12) (2004) 26–36.

[30] Y. Jiang, V. C. Leung, An asymmetric double sided two-way ranging for crystal offset, in: 2007 International Symposium on Signals, Systems and Electronics, 2007, pp. 525–528.

[31] D. D. McCrady, L. Doyle, H. Forstrom, T. Dempsey, M. Martorana, Mobile ranging using low-accuracy clocks, IEEE Transactions on Microwave Theory and Techniques 48 (6) (2000) 938–950.

[32] C. McElroy, D. Neirynck, M. McLaughlin, Comparison of wireless clock synchronization algorithms for indoor location systems, in: 2014 IEEE International Conference on Communications Workshops (ICC), 2014, pp. 157–162.

[33] L. Yunsong, P. Liangfu, A position self-calibration method in multilateration, in: 2017 Forum on Cooperative Positioning and Service (CPGPS), 2017, pp. 101–105.

[34] IEEE Standards, IEEE Std 1139-2008 (Revision of IEEE Std 1139-1999) IEEE Standard Definitions of Physical Quantities for Fundamental Frequency and Time Metrology–Random Instabilities, IEEE, 2009.

[35] R. David, D. R. Brown, Modeling and tracking phase and frequency offsets in low-precision clocks, IEEE Aerospace Conference Proceedings (2015) 1–7.

[36] F. Tirado-Andrés, A. Araujo, Performance of clock sources and their influence on time synchronization in wireless sensor networks, International Journal of Distributed Sensor Networks 15 (9) (2019) 1550147719879372.

[37] M. Youssef, A. Youssef, C. Rieger, U. Shankar, A. Agrawala, Pinpoint: An asynchronous time-based location determination system, in: Proceedings of the 4th International Conference on Mobile Systems, Applications and Services, 2006, pp. 165–176.

[38] K. Yimei, W. Jiawei, A high-precision TOA-based positioning algorithm without the restriction of strict time synchronization for wireless systems, in: 2016 IEEE 13th International Conference on Signal Processing (ICSP), 2016, pp. 1666–1670.

[39] Q. Li, D. Rus, Global clock synchronization in sensor networks, IEEE Transactions on Computers 55 (2) (2006) 214–226.

[40] C. Liu, H. Pang, N. Cao, Research on time synchronization technology of wireless sensor network, in: 2017 International Conference on Cyber-Enabled Distributed Computing and Knowledge Discovery (CyberC), 2017, pp. 391–394.

[41] J. Elson, L. Girod, D. Estrin, Fine-grained network time synchronization using reference broadcasts, ACM SIGOPS Operating Systems Review 36 (SI) (2003) 147–163.

[42] K. L. Noh, E. Serpedin, K. Qaraqe, A new approach for time synchronization in wireless sensor networks: Pairwise broadcast synchronization, IEEE Transactions on Wireless Communications 7 (9) (2008) 3318–3322.

[43] C. Liao, P. Barooah, Time-synchronization in mobile sensor networks from difference measurements, in: 49th IEEE Conference on Decision and Control (CDC), 2010, pp. 2118–2123.

[44] A. Mahmood, R. Exel, H. Trsek, T. Sauter, Clock synchronization over IEEE 802.11 - A survey of methodologies and protocols, IEEE Transactions on Industrial Informatics 13 (2) (2017) 907–922.

[45] Y.-C. Wu, Q. Chaudhari, E. Serpedin, Clock synchronization of wireless sensor networks, IEEE Signal Processing Magazine 28 (1) (2010) 124–138.

[46] N. M. Freris, S. R. Graham, P. Kumar, Fundamental limits on synchronizing clocks over networks, IEEE Transactions on Automatic Control 56 (6) (2010) 1352–1364.

[47] B. Etzlinger, H. Wymeersch, A. Springer, Cooperative synchronization in wireless networks, IEEE Transactions on Signal Processing 62 (11) (2014) 2837–2849.

[48] X. Huan, K. S. Kim, On the practical implementation of propagation delay and clock skew compensated high-precision time synchronization schemes with resource-constrained sensor nodes in multi-hop wireless sensor networks, Computer Networks 166 (2020) 106959.

[49] B. Denis, J.-B. Pierrot, C. Abou-Rjeily, Joint distributed synchronization and positioning in uwb ad hoc networks using toa, IEEE Transactions on Microwave Theory and Techniques 54 (4) (2006) 1896–1911.

[50] J. Zheng, Y.-C. Wu, Joint time synchronization and localization of an unknown node in wireless sensor networks, IEEE Transactions on Signal Processing 58 (3) (2009) 1309–1320.

[51] R. T. Rajan, A. J. Van der Veen, Joint ranging and clock synchronization for a wireless network, 2011 4th IEEE International Workshop on Computational Advances in Multi-Sensor Adaptive Processing, CAMSAP 2011 (2011) 297–300.

[52] S. P. Chepuri, G. Leus, A.-J. Van der Veen, Joint localization and clock synchronization for wireless sensor networks, in: 2012 Conference Record of the Forty Sixth Asilomar Conference on Signals, Systems and Computers (ASILOMAR), IEEE, 2012, pp. 1432–1436.

[53] S. P. Chepuri, R. T. Rajan, G. Leus, A.-J. Van der Veen, Joint clock synchronization and ranging: Asymmetrical time-stamping and passive listening, IEEE Signal Processing Letters 20 (1) (2012) 51–54.

[54] M. R. Gholami, S. Gezici, E. G. Strom, TDOA based positioning in the presence of unknown clock skew, IEEE Transactions on Communications 61 (6) (2013) 2522–2534.

[55] B. Etzlinger, F. Meyer, A. Springer, F. Hlawatsch, H. Wymeersch, Cooperative simultaneous localization and synchronization: A distributed hybrid message passing algorithm, in: 2013 Asilomar Conference on Signals, Systems and Computers, IEEE, 2013, pp. 1978–1982.

[56] B. Etzlinger, C. Pimminger, S. Fischereder, A. Springer, Passive localization and synchronization in the presence of affine clocks, in: 2015 49th Asilomar Conference on Signals, Systems and Computers, IEEE, 2015, pp. 1655–1658.

[57] S. Dwivedi, A. De Angelis, D. Zachariah, P. Händel, Joint ranging and clock parameter estimation by wireless round trip time measurements, IEEE Journal on Selected Areas in Communications 33 (11) (2015) 2379–2390.

[58] F. Ricciato, S. Sciancalepore, F. Gringoli, N. Facchi, G. Boggia, Position and velocity estimation of a non-cooperative source from asynchronous packet arrival time measurements, IEEE Transactions on Mobile Computing 17 (9) (2018) 2166–2179.

[59] R. T. Rajan, A. J. Van der Veen, Joint ranging and synchronization for an anchorless network of mobile nodes, IEEE Transactions on Signal Processing 63 (8) (2015) 1925–1940.

[60] W. Yuan, N. Wu, B. Etzlinger, H. Wang, J. Kuang, Cooperative joint localization and clock synchronization based on gaussian message passing in asynchronous wireless networks, IEEE Transactions on Vehicular Technology 65 (9) (2016) 7258–7273.

[61] B. Etzlinger, F. Meyer, F. Hlawatsch, A. Springer, H. Wymeersch, Cooperative simultaneous localization and synchronization in mobile agent networks, IEEE Transactions on Signal Processing 65 (14) (2017) 3587–3602.

[62] M. Koivisto, M. Costa, J. Werner, K. Heiska, J. Talvitie, K. Leppanen, V. Koivunen, M. Valkama, Joint Device Positioning and Clock Synchronization in 5G Ultra-Dense Networks, IEEE Transactions on Wireless Communications 16 (5) (2017) 2866–2881.

[63] F. Sivrikaya, B. Yener, Time synchronization in sensor networks: a survey, IEEE Network 18 (4) (2004) 45–50.

[64] C. Zucca, P. Tavella, The clock model and its relationship with the Allan and related variances, IEEE Transactions on Ultrasonics, Ferroelectrics, and Frequency Control 52 (2) (2005) 289–295.

[65] R. Schmidt, Multiple emitter location and signal parameter estimation, IEEE Transactions on Antennas and Propagation 34 (3) (1986) 276–280.

[66] J. Winter, C. Wengerter, High resolution estimation of the time of arrival for GSM location, in: VTC2000-Spring. 2000 IEEE 51st Vehicular Technology Conference Proceedings (Cat. No.00CH37026), Vol. 2, 2000, pp. 1343–1347.

[67] Xinrong Li, K. Pahlavan, Super-resolution TOA estimation with diversity for indoor geolocation, IEEE Transactions on Wireless Communications 3 (1) (2004) 224–234.

[68] N. Alsindi, X. Li, K. Pahlavan, Analysis of time of arrival estimation using wideband measurements of indoor radio propagations, IEEE Transactions on Instrumentation and Measurement 56 (5) (2007) 1537–1545.

[69] R. Roy, T. Kailath, ESPRIT-estimation of signal parameters via rotational invariance techniques, IEEE Transactions on Acoustics, Speech, and Signal Processing 37 (7) (1989) 984–995.

[70] D. Humphrey, M. Hedley, Super-resolution time of arrival for indoor localization, in: 2008 IEEE International Conference on Communications, 2008, pp. 3286–3290.

[71] V. U. Prabhu, D. Jalihal, An improved ESPRIT based time-of-arrival estimation algorithm for vehicular OFDM systems, in: VTC Spring 2009-IEEE 69th Vehicular Technology Conference, 2009, pp. 1–4.

[72] D. Oh, S. Kim, S.-H. Yoon, J.-W. Chong, Two-dimensional ESPRIT-like shift-invariant TOA estimation algorithm using multi-band chirp signals robust to carrier frequency offset, IEEE Transactions on Wireless Communications 12 (7) (2013) 3130–3139.

[73] S. Kim, D. Oh, J. Lee, Joint DFT-ESPRIT estimation for TOA and DOA in vehicle FMCW radars, IEEE Antennas and Wireless Propagation Letters 14 (2015) 1710–1713.

[74] M. Driusso, F. Babich, F. Knutti, M. Sabathy, C. Marshall, Estimation and tracking of LTE signals time of arrival in a mobile multipath environment, in: 2015 9th International Symposium on Image and Signal Processing and Analysis (ISPA), 2015, pp. 276–281.

[75] B. H. Fleury, M. Tschudin, R. Heddergott, D. Dahlhaus, K. I. Pedersen, Channel parameter estimation in mobile radio environments using the SAGE algorithm, IEEE Journal on Selected Areas in Communications 17 (3) (1999) 434–450.

[76] C.-C. Chong, D. I. Laurenson, C. M. Tan, S. McLaughlin, M. A. Beach, A. R. Nix, Joint detection-estimation of directional channel parameters using the 2-D frequency domain SAGE algorithm with serial interference cancellation, in: 2002 IEEE International Conference on Communications. Conference Proceedings. ICC 2002 (Cat. No. 02CH37333), Vol. 2, 2002, pp. 906–910.

[77] M. Noschese, F. Babich, M. Comisso, C. Marshall, On the performance of SAGE algorithm for ToA estimation in dual-band OFDM systems, in: 2018 IEEE 29th Annual International Symposium on Personal, Indoor and Mobile Radio Communications (PIMRC), 2018, pp. 1–6.

[78] A. Jakobsson, A. L. Swindlehurst, P. Stoica, Subspace-based estimation of time delays and Doppler shifts, IEEE Transactions on Signal Processing 46 (9) (1998) 2472–2483.

[79] J. Vidal, M. Nájar, R. Játiva, High resolution time-of-arrival detection for wireless positioning systems, in: Proceedings IEEE 56th Vehicular Technology Conference, Vol. 4, 2002, pp. 2283–2287.

[80] C. Falsi, D. Dardari, L. Mucchi, M. Z. Win, Time of arrival estimation for UWB localizers in realistic environments, EURASIP Journal on Advances in Signal Processing 2006 (2006) 1–13.

[81] S. A. Golden, S. S. Bateman, Sensor measurements for Wi-Fi location with emphasis on time-of-arrival ranging, IEEE Transactions on Mobile Computing 6 (10) (2007) 1185–1198.

[82] T. Camp, J. Boleng, V. Davies, A survey of mobility models for ad hoc network research, Wireless communications and mobile computing 2 (5) (2002) 483–502.

[83] F. Gustafsson, F. Gunnarsson, Mobile positioning using wireless networks: possibilities and fundamental limitations based on available wireless network measurements, IEEE Signal Processing Magazine 22 (4) (2005) 41–53.

[84] R. G. Brown, P. Y. Hwang, Introduction to random signals and applied Kalman filtering: with MATLAB exercises, J Wiley & Sons, 2012.

[85] B. Ristic, S. Arulampalam, N. Gordon, Beyond the Kalman filter: Particle filters for tracking applications, Artech House, 2004.

[86] R. Schneider, C. Georgakis, How to NOT make the extended Kalman filter fail, Industrial and Engineering Chemistry Research 52 (9) (2013) 3354–3362.

[87] S. J. Julier, J. K. Uhlmann, New extension of the Kalman filter to nonlinear systems, in: I. Kadar (Ed.), Signal Processing, Sensor Fusion, and Target Recognition VI, Vol. 3068, International Society for Optics and Photonics, SPIE, 1997, pp. 182 – 193.

[88] S. J. Julier, J. K. Uhlmann, Unscented filtering and nonlinear estimation, Proceedings of the IEEE 92 (3) (2004) 401–422.

[89] E. A. Wan, R. Van Der Merwe, The unscented Kalman filter for nonlinear estimation, in: Proceedings of the IEEE 2000 Adaptive Systems for Signal Processing, Communications, and Control Symposium (Cat. No. 00EX373), 2000, pp. 153–158.

[90] E. A. Wan, R. Van der Merwe, The Unscented Kalman Filter, John Wiley & Sons, 2002, Ch. 7, pp. 221–280.

[91] N. J. Gordon, D. J. Salmond, A. F. Smith, Novel approach to nonlinear/non-Gaussian Bayesian state estimation, IEE Proceedings F (Radar and Signal Processing) 140 (2) (1993) 107–113.

[92] A. Doucet, N. de Freitas, N. Gordon (Eds.), Sequential Monte Carlo Methods in Practice, 1st Edition, Statistics for Engineering and Information Science, Springer-Verlag, 2001.

[93] M. S. Arulampalam, S. Maskell, N. Gordon, T. Clapp, A tutorial on particle filters for online nonlinear/non-Gaussian Bayesian tracking, IEEE Transactions on Signal Processing 50 (2) (2002) 174–188.

[94] R. Van der Merwe, A. Doucet, N. De Freitas, E. Wan, The Unscented Particle Filter, in: Proceedings of the 13th International Conference on Neural Information Processing Systems, NIPS'00, MIT Press, 2000, p. 563–569.

[95] D. Simon, Optimal state estimation: Kalman, H infinity, and nonlinear approaches, John Wiley & Sons, 2006.

[96] L. Banin, O. Bar-Shalom, N. Dvorecki, Y. Amizur, Scalable Wi-Fi Client Self-Positioning Using Cooperative FTM-Sensors, IEEE Transactions on Instrumentation and Measurement 68 (10) (2019) 3686–3698.

[97] B. K. Horn, Doubling the accuracy of indoor positioning: Frequency diversity, Sensors 20 (5) (2020) 1489.

[98] Decawave, Application abstract: Aps011. Sources of Error in DW1000 Based Two-Way Ranging (TWR) Schemes (2014) 1–21.

[99] N. Garcia, H. Wymeersch, E. G. Larsson, A. M. Haimovich, M. Coulon, Direct localization for massive MIMO, IEEE Transactions on Signal Processing 65 (10) (2017) 2475–2487.

[100] G. H. Golub, C. F. Van Loan, Matrix computations, 4th Edition, Johns Hopkins University Press, 2013.

[101] P. Tichavsky, C. H. Muravchik, A. Nehorai, Posterior Cramér-Rao bounds for discrete-time nonlinear filtering, IEEE Transactions on Signal Processing 46 (5) (1998) 1386–1396.